Modeling and Vibration Feedback Control of Rotating Tapered Composite Thin-Walled Blade

Jae Kyung Shim, Sungsoo Na*

Department of Mechanical Engineering Korea University Anam-dong, Sungbuk-ku, Seoul 136-701, Korea

This paper addresses the problem of the modeling and vibration control of tapered rotating blade modeled as thin-walled beams and incorporating damping capabilities. The blade model incorporates non-classical features such as anisotropy, transverse shear, secondary warping and includes the centrifugal and Coriolis force fields. For the rotating blade system, a thorough validation and assessment of a number of non-classical features including the taper characteristics is accomplished. The damping capabilities are provided by a system of piezoactuators bonded or embedded into the structure and spread over the entire span of the beam. Based on the converse piezoelectric effect, the piezoactuators produce a localized strain field in response to a voltage and consequently, a change of the dynamic response characteristics is induced. A velocity feedback control law relating the piezoelectrically induced transversal bending moment at the beam tip with the appropriately selected kinematical response quantity is used and the beneficial effects upon the closed-loop dynamic characteristics of the blade are highlighted.

Key Words : Vibration Control, Piezoactuator, Rotating Blade, Thin-Walled Beam, Composite Materials

1. Introduction

The study of the eigenvibration response of rotating beams is an important prerequisite in the design of helicopter, tilt rotor aircraft, and turbomachinery. An important step toward the rational design of modern rotor blades and propellers consists of the development of analytical models that are capable of accurately predicting their dynamic behaviors. Moreover, in order to enhance their dynamic behaviors and avoid vibration-induced fatigue failure, new technologies have to be implemented. One of the ways to accomplish such goals consists of the incorporation of adaptive materials into the host structure, which is able to respond actively to changing conditions. In contrast to traditional passive structures, in a structure featuring adaptive capabilities, the natural frequencies, damping, and mode shapes can be tuned to avoid structural resonance and enhance dynamic response characteristics. In addition, due to the nature of intelligent structures that feature a highly distributed networks of sensors and actuators, more encompassing control schemes that are impractical when a small number of actuators are used, would be possible to be implemented. For helicopter and tilt rotor aircraft, the incorporation of adaptive materials technology for vibration control could result in significant increases in comfort, range, life, etc. In this sense, piezoelectric materials are excellent candidates for the roles of sensors and actuators.

In this paper, a study of the in-plane (lagging) and transverse to the plane of rotation (flapping) free vibration of rotating beams featuring non-uniform cross sections is addressed. Then, by

* Corresponding Author,
E-mail : nass@korea.ac.kr
TEL : +82-2-3290-3370; **FAX** : +82-2-926-9290
Department of Mechanical Engineering Korea University Anam-dong, Sungbuk-ku, Seoul 136-701, Korea.
(Manuscript **Received** August 14, 2002; **Revised** December 26, 2002)

incorporating the capability referred to as induced strain actuation a control of flapping vibration is carried out. The damping capability is achieved through the converse piezoelectric effect that consists of the generation of localized strains in response to an applied voltage. The induced strain field produces, in turn, an adaptive change in the dynamic response characteristics of the structure.

Under consideration is a rotating blade which is modeled as a thin walled beam of nonuniform cross section. Herein, the blade is considered to be tapered both in width and depth.

Although of an evident importance, to the best of the author's knowledge, no such studies can be found in the specialized literature. To the best of the author's knowledge the free bending vibration problem of rotating tapered beams was done within the solid beam model only. Some results addressing the issue of uncontrolled rotating blades modeled as solid beam and restricted to flapping vibration can be found e.g. in the papers by Bazoune et al. (1999), Khulief and Bazoune (1992), and J. Park and H. Yoo (1996). In the other context, Kim and Yoo (2002) investigated the coupling motion between inplane motion and bending motion in plate model. The results obtained herein constitute a generalization of the ones previously obtained in the papers by Na and Librescu (1999), Song and Librescu (1997) and Librescu et al. (1997).

2. General Considerations

In this paper, the case of straight untwisted nonuniform blade rotating with constant angular velocity is considered. Figure 1(a) shows the geometric configuration and the typical cross-section of a blade considered here along with the associated system of coordinates. The inertial system of coordinates X-Y-Z is assumed to be attached to the center of the hub O, and the origin of the rotating axis system x-y-z is located at the blade root at an offset R_0 of the rotation axis fixed in space. R_0 also denotes the radius of the hub in which the blade is mounted and which rotates about its polar axis through the origin O. By **i**, **j**, **k** and **I**, **J**, **K**, we define the unit vectors associated with the coordinate systems x-y-z and X-Y-Z, respectively. In addition, a local (surface) coordinate system s-z-n associated with the beam is considered.

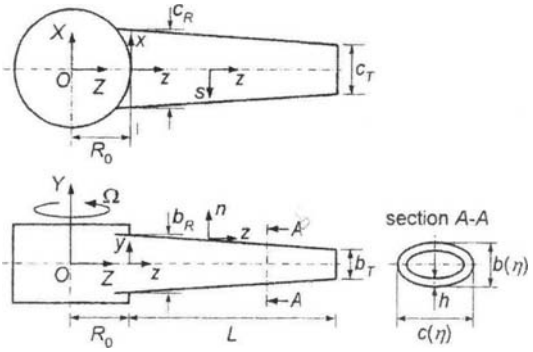

Fig. 1(a) Rotating blade and coordinates used

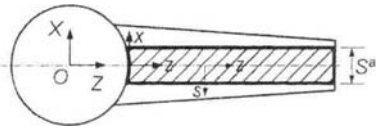

Fig. 1(b) Distribution of the piezoactutor (thickness t^a=0.0002m, width S^a=0.089m)

Within the present work, it is assumed that the presetting and sweep angles of the blade are zero. It is further assumed that the rotation takes place in the X-Z plane with the constant angular velocity $\Omega(\Omega\mathbf{J}\equiv\Omega\mathbf{j})$, the spin axis being along the Y-axis. The structural model corresponds to a thin/thick-walled beam. In this context the case of a single-cell thin-walled beam of nonuniform closed-sections is considered, where the spanwise, the z-coordinate axis coincides with a straight unspecified reference axis. It is assumed that the piezoactuator layers are distributed over the entire beam span and that the polarization is in their thickness direction.

The equations of rotating thin-walled beams are based upon the following statements (Song and Librescu 1997, Na and Librescu 2000a): (i) The original cross-section of the beam is preserved; (ii) the transverse shear effects are taken into account; (iii) the circumferential stress resultant Nss (i.e., the hoop stress resultant) is negligibly small when compared to the remaining

ones; (iv) doubly-tapered beam in both the horizontal and vertical planes are considered; (v) the case of a bi-convex beam cross-section profile is adopted; and (vi) both the materials of the host structure and of the piezoactuators exhibit transversely-isotropic properties, the surface of isotropy being parallel at each point to the mid-surface of the beam.

By virtue of the assumption (iv), the following linear distribution of the chord $c(\eta)$ and height $b(\eta)$ of the mid-line cross-section profiles along the wing span (Librescu et al., 1994), is considered.

$$\begin{Bmatrix} c(\eta) \\ b(\eta) \end{Bmatrix} = [1-\eta(1-\sigma)] \begin{Bmatrix} c_R \\ b_R \end{Bmatrix} \tag{1}$$

Herein $\sigma \equiv c_T/c_R (\equiv b_T/b_R)$ denotes the taper ratio, $\eta = z/L$ is the dimensionless spanwise coordinate ($\eta \in [0, 1]$), where L denotes the wing semi-span, $c(\eta)$ and $b(\eta)$ denote the local wing chord and height, respectively, while subscripts R and T identify the wing characteristics at the root and tip cross-sections, respectively. Moreover, the radius of curvature of the circular arc associated with the midline contour at section η along the wing span is expressed as

$$R(\eta) = [1-\eta(1-\sigma)] R_R \tag{2}$$

As the result of the transversely isotropic property of both the piezoactuators and of the host structure, an exact decoupling of transverse bending (flapping-expressed in terms of variables v_0 and θ_x), chordwise bending (lagging, u_0 and θ_y), twist (Θ), and axial (w_0) motions are induced. Each of kinematic variables $u_0(z;t)$, $v_0(z;t)$, $w_0(z;t)$, $\theta_x(z;t)$, $\theta_y(z;t)$, and $\Theta(z;t)$ represent three translations in the x, y, and z direction and three rotations about the x-, y-, and z-axis, respectively. For the problem studied herein, only flapping and lagging motions will be considered. However, since secondary warping induces transverse bending, this effect will also be incorporated. Finally, it is assumed that the electric field vector E_i is represented in terms of its component E_3 in the n-direction only.

3. The Dynamic Equations of Adaptive Rotating Cantilevered Beams

Hamilton's variational principle is applied in order to obtain the equations of motion of adaptive rotating beams and the associated boundary conditions. By virtue of this principle, of all displacements $v_i \equiv v_i(x, y, z; t)$ that satisfy the boundary conditions (BCs) $v_i = \bar{v}_i$ over $\mathcal{Q}$ and also fulfill the condition $\delta v_i = 0$ at $t = t_0$ and $t = t_1$, where t_0 and t_1 are two arbitrary instants of time, the actual ones fulfill the following variational equation.

$$\delta J = \int_{t_0}^{t_1} \left[\int_\tau \sigma_{ij} \delta \varepsilon_{ij} d\tau - \delta K - \int_{\mathcal{Q}} \bar{s}_i \delta v_i d\mathcal{Q} - \int_\tau \rho H_i \delta v_i d\tau \right] dt = 0 \tag{3}$$

where

$$K = \frac{1}{2} \int_\tau \rho (\dot{\mathbf{R}} \cdot \dot{\mathbf{R}}) \, d\tau \tag{4}$$

denotes the kinetic energy, $d\tau (\equiv dndsdz)$ denotes the differential volume element, $\bar{s}_i (\equiv \bar{\sigma}_{ij} n_j)$ denote the prescribed components of the stress vector on a surface element of the undeformed body characterized by the outward normal components n_i, H_i denote the components of the body forces, $\mathcal{Q}$ denotes the external area of the body over which the stresses are prescribed, ρ denotes the mass density, an overtilde sign identifies a prescribed quantity, and δ denotes the variation operator. In order to evaluate the quantities entering the energy functional, the position vector $\mathbf{R} (\equiv \mathbf{R}(x, y, z; t))$ of a deformed point of the beam is defined as:

$$\mathbf{R} = \mathbf{R}_0 + \mathbf{r} + \boldsymbol{\Delta} \tag{5}$$

In Eq. (5), $\mathbf{r} (\equiv x\mathbf{i} + y\mathbf{j} + z\mathbf{k})$ defines the undeformed position of a point measured in the beam coordinate system and $\boldsymbol{\Delta} (\equiv u\mathbf{i} + v\mathbf{j} + w\mathbf{k})$ denotes the displacement vectors of the points of the blade, while $\mathbf{R}_0 = R_0\mathbf{k}$. We will also make use of the equations expressing the time derivatives of unit vectors, namely $(\dot{\mathbf{i}}, \dot{\mathbf{j}}, \dot{\mathbf{k}}) = (-\Omega\mathbf{k}, 0, \Omega\mathbf{i})$, and the expressions of components R_i of the position vector of a deformed point of the blade, as well as those of velocity V_i and acceleration a_i

components. Their distribution throughout the beam is (Song and Librescu 1997; Na and Librescu 2000a)

$$V_1=\dot{u}+(R_0+z+w)\,\Omega \tag{6}$$

$$V_2=\dot{v} \tag{7}$$

$$V_3=\dot{w}-(x+u)\,\Omega \tag{8}$$

and

$$a_1=\ddot{u}+\underline{2\dot{w}\Omega}-\underline{\underline{(x+u)\,\Omega^2}} \tag{9}$$

$$a_2=\ddot{v} \tag{10}$$

$$a_3=\ddot{w}-\underline{2\dot{u}\Omega}-\underline{\underline{(R_0+z+w)\,\Omega^2}} \tag{11}$$

respectively. In Eqs. (6)-(11), as well as in the forthcoming ones, the terms overscored by a single and double bars identify the Coriolis and centrifugal acceleration terms, respectively. In addition, u, v and w denote the components of the three-dimensional displacement vector defined in terms of one-dimensional generalized displacement, which can be expressed as

$$u(x, y, z; t)=\underline{\underline{u_0(z; t)}}-y\Theta(z; t) \tag{12}$$

$$v(x, y, z; t)=v_0(z; t)+x\Theta(z; t) \tag{13}$$

$$\begin{aligned} w(n, s, z; t)=&w_0(z; t)\\ &+\underline{\underline{x(s)\,\theta_y(z; t)}}+\underline{y(s)\,\theta_x(z; t)}\\ &-F_w(s)\,\Theta'(z; t)\\ &+n\left[\frac{dy}{ds}\underline{\theta_y(z; t)}\right.\\ &\left.+\frac{dx}{ds}\underline{\theta_x(z; t)}-a(s)\,\Theta'(z; t)\right] \end{aligned} \tag{14}$$

In Eqs. (12) and (14) the terms overscored by one and two solid lines belong to the flapping and lagging motions, respectively, where primes denote differentiation with respect to the longitudinal z-coordinate. The remaining terms in these expressions are associated with the axial warping and twist motions.

The first integral in Eq. (3) should be considered in the sense

$$\int_t(\cdot)\,d\tau=\int_0^L\oint\sum_{k=1}^{r+p}\int_{h_{k-1}}^{h_k}(\cdot)\,dn ds dz \tag{15}$$

where $r+p$ denotes the total number of layers, $\oint(\cdot)\,ds$ denotes the integral around the circumference of the mid-line cross section of the beam, and L denotes the span of the beam.

4. The Governing System

The governing equations of nonuniform rotating blades can be represented in terms of displacement quantities. This can be done by expressing the stress-resultants and stress-couples in the equations of motion in terms of displacement variables. These equations that can be found in the papers by Song and Librescu (1997), are not displayed here.

It should be stressed, however, that even by neglecting Coriolis' effects, for a general type of anisotropy of the layer materials (i.e. of the host structure, of the actuator patches, or of both of them), the system of governing equations result in a complete coupled form. However, for the type of anisotropy considered herein, (i.e. of transverse isotropy) an exact split of the governing system of equations and of the associated BCs into four uncoupled subsystems arises. In the sequence considered above, the subsystems of equations govern the coupling between chordwise shear and flapwise bending, as well as extension and twist motions, respectively. These subsystems of equations are labelled as system (A) and (B), respectively.

Since the analysis is confined here to rotating blades featuring lagging and flapping motions only, the associated governing equations and BCs for cantilevered beams are given explicitly as follows. Equations involving the coupling chordwise bending-chordwise shear (i.e. coupling (A)) are

$$\begin{aligned} \delta u_0:\ &[a_{44}(u_0'+\theta_y)]'+\Omega^2\{[P(z)]\,u_0'\}'\\ &\underline{-2b_1\Omega\dot{w}_0'}+\underline{b_1\Omega^2u_0}-b_1\ddot{u}_0=0 \end{aligned} \tag{16}$$

$$\begin{aligned} \delta\theta_y:\ &(a_{22}\theta_y')'-\underline{a_{44}(u_0'+\theta_y)}\\ &-I_{yy}(\ddot{\theta}_y-\Omega^2\theta_y)=0 \end{aligned} \tag{17}$$

and the BCs at $z=0$ are

$$u_0=0 \tag{18}$$

$$\theta_y=0 \tag{19}$$

and the BCs at $z=L$ are

$$\delta u_0:\ a_{44}(u_0'+\theta_y)=0 \tag{20}$$

$$\delta\theta_y:\ a_{22}\theta_y'=\hat{M}_y \tag{21}$$

Herein the coefficients a_{ij}, I_{ij}, and b_i denote stiffness, mass, and structural properties, respectively, whose expressions are displayed in Appendix, while $\hat{M}_y$ denotes piezoelectrically induced moment in the lagging direction. The equations involving the coupling flapwise shear-flapwise bending (i.e. coupling(B)) are

$$\delta v_0 : [a_{55}(v_0' + \theta_x)]' + \Omega^2\{[P(z)]v_0'\}' - b_1\ddot{v}_0 + p_y = 0 \tag{22}$$

$$\delta\theta_x : (a_{33}\theta_x')' - a_{55}(v_0' + \theta_x) - I_{xx}(\ddot{\theta}_x - \overline{\Omega^2\theta_x}) - 2I_{xx}^0\Omega\dot{\Theta} = 0 \tag{23}$$

and the BCs at $z=0$ are

$$v_0 = 0 \tag{24}$$

$$\theta_x = 0 \tag{25}$$

and the BCs at $z=L$ are

$$\delta v_0 : a_{55}(v_0' + \theta_x) = 0 \tag{26}$$

$$\delta\theta_x : a_{33}\theta_x' = \hat{M}_x. \tag{27}$$

Herein the coefficients a_{ij}, I_{ij}, I_{ij}^0 and b_i denote stiffness, mass, and structural properties, respectively, whose expressions are displayed in Appendix A, while $\hat{M}_x$ denotes piezoelectrically induced moment in the flapping direction. Elimination of $a_{44}(u_0' + \theta y)$ and $a_{55}(v_0' + \theta_x)$ from the group of equations (16), (17), (20), (22-23), and (26) respectively, followed by consideration of $\theta_x = -v_0'$ and $\theta_y = -u_0'$, results in the non-shearable counterpart of the two groups of equations, (A) and (B). These are as follows.

Classical counterpart of the equation group (A):

$$\delta u_0 : (a_{22}u_0'')'' - \Omega^2\{[P(z)]u_0'\}' + 2\overline{b_1\Omega\dot{v}_0'} - \overline{b_1\Omega^2 u_0} + b_1\ddot{u}_0 - [I_{yy}(\ddot{u}_0' - \overline{\Omega^2 u_0'})]' = 0 \tag{28}$$

and the BCs at $z=0$ are

$$u_0 = 0 \tag{29}$$

$$u_0' = 0 \tag{30}$$

and the BCs at $z=L$ are

$$\delta u_0 : [a_{22}u_0'']' - I_{yy}(\ddot{u}_0' - \overline{\Omega^2 u_0'}) = 0 \tag{31}$$

$$\delta u_0' : a_{22}u_0 = \hat{M}_y \tag{32}$$

Non-shearable counterpart of the equation group (B):

$$\delta v_0 : [a_{33}v_0'']'' - \Omega^2\{[P(z)]v_0'\}' - [I_{xx}(v_0' - \overline{\Omega^2 v_0'})]' + b_1\ddot{v}_0 = 0 \tag{33}$$

and the BCs at $z=0$ are

$$v_0 = 0 \tag{34}$$

$$v_0' = 0 \tag{35}$$

and the BCs at $z=L$ are

$$\delta v_0 : [a_{33}v_0'']' - I_{xx}(\ddot{v}_0' - \overline{\Omega^2 v_0'}) + I_{xx}^0\Omega\dot{\Theta} = 0 \tag{36}$$

$$\delta v_0' : a_{33}v_0 = \hat{M}_x \tag{37}$$

In Eqs. (16), (22), (28) and (33) $P(z)$ is obtained as

$$P(z) = \int_z^L b_1(z)(R_0 + z)\,dz \tag{38}$$

As is readily seen, the coupling between the lagging-extension and flapping- twist motions induced by the Coriolis effect, occurs also within the classical beam model. Consistent with the number of four boundary conditions, the governing equations associated with lagging and flapping are each of fourth order. This feature is valid for both shear-deformable and non-shearable rotating beams. It should be remarked that in the light of the actuator configuration, the piezoelectrically-induced stress-resultant and stress-couples are independent on the z-coordinate. As a result, in the governing equations their contribution is immaterial while in the BCs they intervene as non-homogeneous terms only. This feature renders the control to be accomplished via the piezoelctrically induced bending moments at the beam tip (Librescu et al. 1993, 1997; Na and Librescu 2000a, 2000b). However, due to the shape of the cross-section beam contour, only the control of flapping motion can be accommodated.

5. The Control Law

One of the possibilities of generating bending control moment at the beam tip is via the implementation into the structure of piezoactuators and the use of the converse effect featured by these devices. As shown (see e.g. Tzou, 1993; Librescu et al. 1993, 1996, 1997), piezoactuators

featuring in-plane isotropic properties, spread over the entire span of the beam, bonded symmetrically on the outer and inner faces of the beam but activated out-of-phase, generates a bending moment at the beam tip in response to the applied electric field. In the previously displayed equations, due to the special distribution of piezoactuators, it was shown that the piezoelectrically induced moment $\hat{M}_x$ intervenes solely in the BCs associated with the bending motion, prescribed at the beam tip and, hence, it plays the role of the boundary moment control.

The damping nature of the rotating beam is introduced by requiring the applied electric field E_3 to be related to one of the mechanical quantities characterizing its dynamic response. As a result, a number of control laws can be implemented.

Within the adopted feedback control law the piezoelectrically induced bending moment $\hat{M}_x$ at the blade tip, is expressed as

$$\hat{M}_x(L) = k_v \dot{\theta}_x(L) \tag{39}$$

Herein k_v denotes the velocity feedback gain.

6. Numerical Illustrations and Discussion

The distribution of the piezoactuator is displayed in Fig. 1(b) while the properties of the PZT-4 piezoceramic are: (Berlincourt et al. 1964).

ElasticCoefficients (N/m^2):
C_{11}=3.531e11 C_{12}=1.975e11 C_{13}=1.886e11
C_{33}=2.921e11 C_{44}=6.502e10
Density ($N\,sec^2/m^4$): ρ=1.22824e5
Piezoelectric Coefficients ($N \cdot V/m$):
e_{31}=−5.2 e_{33}=15.1 e_{15}=12.7

For the free vibration problem, it is necessary to solve the closed-loop eigenvalue problem. To this end, the unknown variables are represented in a generic form as

$$F(z, t) = \overline{F}(z)\exp(\lambda t) \tag{40}$$

Use of the representation of Eq. (40) in Eqs. (16) through (21) associated with lagging motion, and in Eqs. (22) through (27), associated with the flapping, motion, results in two differential eigenvalue problems in terms of $\overline{u_0}(z)$ and $\overline{\theta_y}(z)$ on one hand, and in terms of $\overline{v_0}(z)$ and $\overline{\theta_x}(z)$ on the other hand. Because the differential eigenvalue problem does not admit a closed-form solution, it is necessary to discretize it in the spatial variable. Because this is a non-self-adjoint problem, the indicated discretization procedure is the Galerkin's method, which to expanding $\overline{u_0}(z)$, $\overline{v_0}(z)$, $\overline{\theta_x}(z)$, and $\overline{\theta_y}(z)$ in series of trial functions satisfying all boundary conditions, multiplying Eqs. (16), (17), (22) and (23) by the same trial functions, in sequence, integrating over the structure and obtaining a non-symmetric algebraic eigenvalue problem. The difficulty with this approach lies in the requirement that the trial functions satisfy both the geometric and the natural boundary conditions. The difficulty can be circumvented by using a modified Galerkin's method, whereby the discretization process is carried out directly in the extended Hamilton's principle. (Librescu et al. 1997) In the case $k_v \neq 0$, the solution of the algebraic eigenvalue problem yields the closed-loop eigenvalues

$$(\lambda_r, \bar{\lambda}_r) = \sigma_r \pm i\omega_{dr} \qquad r = 1, 2, \cdots, n \tag{41}$$

which depend on the feedback control gain k_v, where σ_r is a measure of the damping in the r-th mode, while ω_{dr} is the r-th frequency of damped oscillations. The damping factor in the r-th mode results as

$$\zeta_r = -\frac{\sigma_r}{(\sigma_r^2 + \omega_{dr}^2)^{\frac{1}{2}}} \tag{42}$$

Several steps aiming at solving the open/closed loop eigenvalue problem are shown in Appendix B.

In Table 1, numerical results obtained by using the present modeling method are compared with available predictions in literatures, which shows the fundamental flapping frequency obtained in the context of Euler-Bernoulli beam model, for two extreme values of the hub ratio $r_0 (\equiv R_0/L)$. The displayed frequencies have been obtained by Hodges (1981) via the asymptotic method, while the one by Du et al. (1994) via the Frobenius and

Table 1 Comparison of the natural frequencies in flapping vibration

Ω	r_0	Hodges(1981)	Du et al. (1994) (Exact)	Present
0	0	3.51602	3.51602	3.51602
	1	3.51602	3.51602	3.51602
5	0	6.4450	6.44954	6.44958
	1	8.93210	8.94036	8.94050
10	0	11.1956	11.2023	11.2026
	1	16.5905	16.6064	16.6066

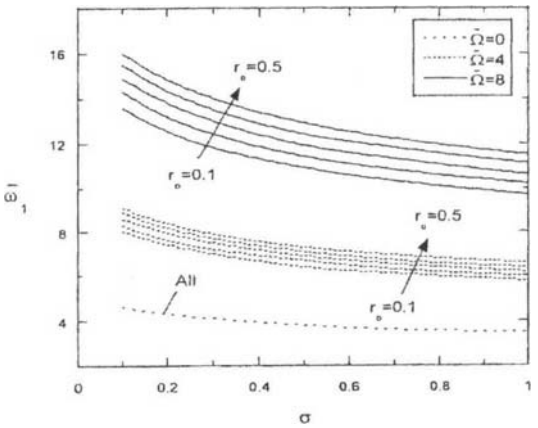

Fig. 2 Variation of the fundamental dimensionless flapping frequency with the taper ratios for selected values of the rotational speed $\bar{\Omega}$ and hub ratio r_0

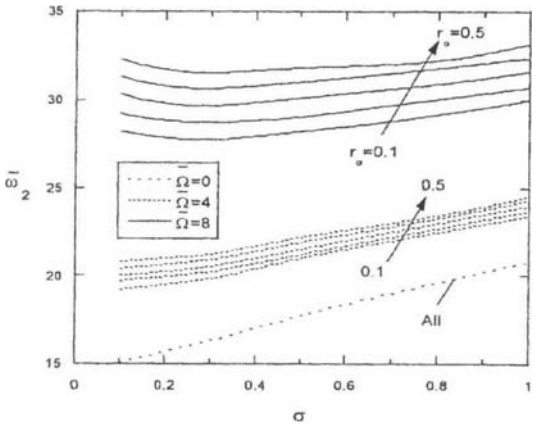

Fig. 3 The counterpart of Fig. 2 for the second flapping frequency

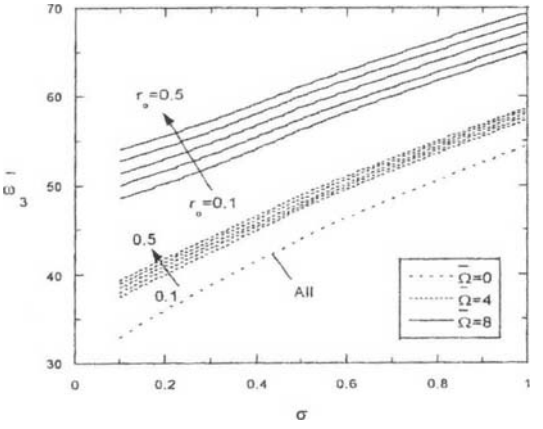

Fig. 4 The counterpart of Fig. 2 for the third flapping frequency

power series technique. It should be remarked that the equations of rotating thin-walled beams are formally similar to the ones corresponding to a solid beam. The difference these two models occurs only in the proper expression of cross-sectional stiffness quantities and mass terms. For this reason, use of dimensionless parameters in which these quantities are absorbed will enable one to obtain universal results valid for both solid and thin-walled rotating beams. Herein the normailized angular velocity $\bar{\Omega}$ and eigenfrequency $\bar{\omega}_i$ are defined as $(\bar{\Omega}, \bar{\omega}_i) = (\Omega, \omega_i)(b_1 L^4/a_{33})^{1/2}$.

In Figs. 2-4, there are emphasized the effects of the taper parameter σ considered in conjunction with that of the blade normalized rotational speed $\bar{\Omega}$ and of the hub ratio r_0 on dimensionless eigenfrequencies $\bar{\omega}_i$. From Figs. 2-4, it becomes evident that as the beam taper increases (i.e when σ decreases), the first natural frequency increases whereas the second and the third ones decrease. However, in Fig. 3 it becomes apparent that with the increase of $\bar{\Omega}$ and decrease of σ there is a critical taper ratio for a beam rotating at relatively high speed for which the decay of the natural frequency with the decrease of σ stops, and a slight change of trend is manifested. A general remark emerging from Figs. 2-4 is that the stiffening effect due to beam rotation contributes to the increase of natural frequencies for all taper ratios. Moreover, the hub radius has a beneficial effect of increasing the eigenfrequencies, especially at higher rotational speeds where the effect appears to be more prominent.

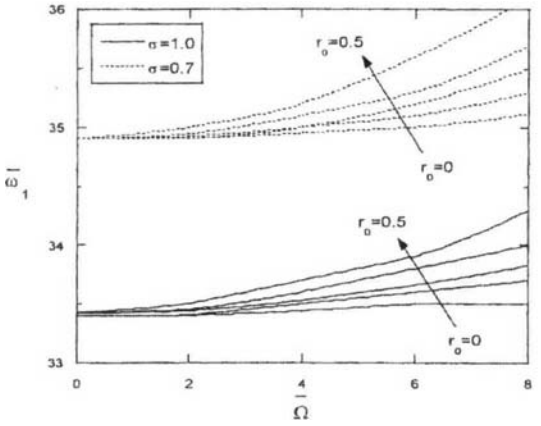

Fig. 5 Fundamental lagging frequency (dimensionless) vs. $\overline{\Omega}$ for selected values of the taper ratio and hub ratio (classical beam model)

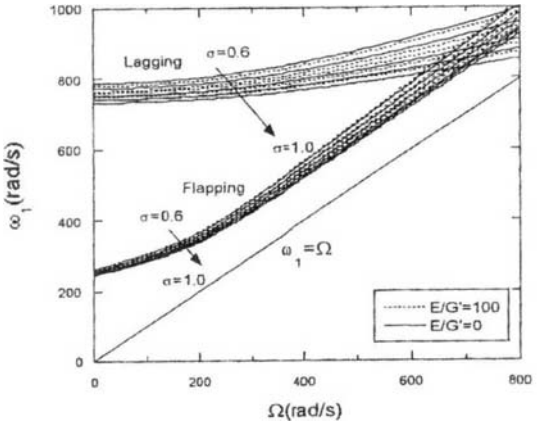

Fig. 6 Fundamental flapping and lagging frequencies vs. rotating speed for selected values of the taper ratio ($E/G'=100$, $r_0=0.1$)

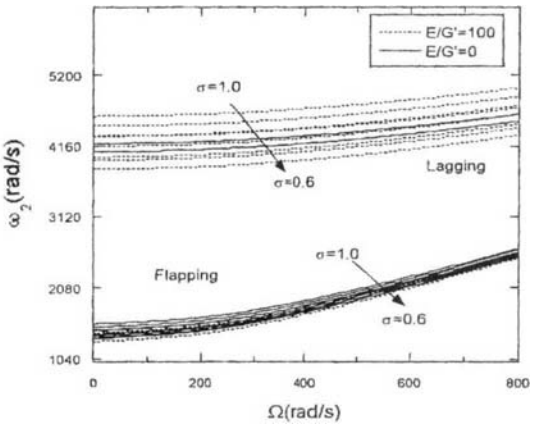

Fig. 7 The counterpart of Fig. 6 for the second frequencies in flapping and lagging. The effects of transverse shear are also emphasized

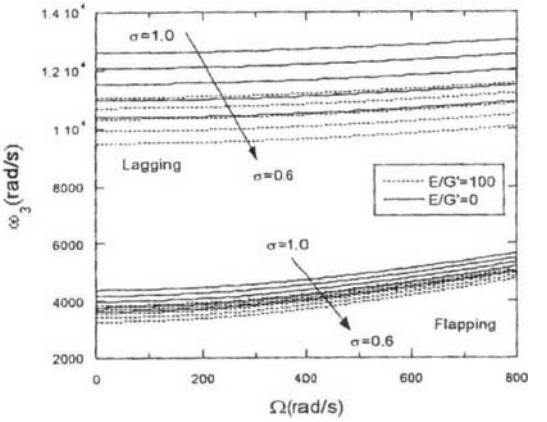

Fig. 8 The counterpart of Fig. 6 for the third frequencies in flapping and lagging

In Fig. 5 there are depicted the implications of the rotational speed considered in conjunction with these of the taper ratios and hub ratios on the dimensionless first natural frequency in lagging. Since the frequencies in lagging are higher than their counterparts in flapping, the stiffening due to the centrifugal effect is weaker than that exerted on flapping frequencies. The same trend also emerges from Fig. 6 where the Campbell diagrams were completed to also include the effect of the beam taper ratio. Figures 7 and 8 constitute the counterparts for the second and third frequencies in flapping-lagging, of Fig. 6, where in addition the implications of transverse shear flexibility are emphasized. These reveal that: (i) the effect of rotation is much more reduced for the second and third flap frequencies than for the first one; (ii) the effects of σ and of transverse shear are much stronger for the lagging frequencies (second and third), than for their flapping frequencies counterparts.

As was already mentioned, the shape of the cross-section profile considered in conjunction with implementation of the control methodology enables one to control the flapwise motion only. With this in mind, Figs. 9-11 depict the variation of the first three closed-loop eigenfrequencies with the dimensionless velocity feedback gain for

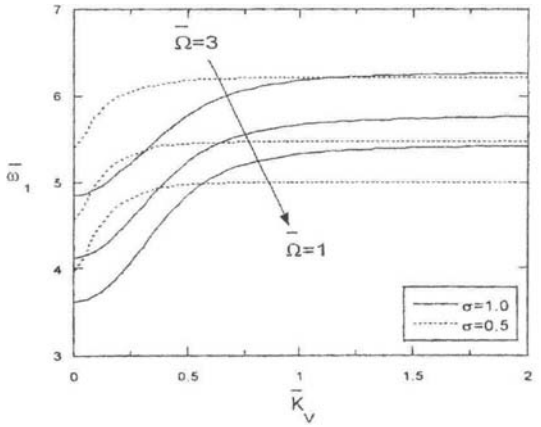

Fig. 9 Closed loop fundamental flapping frequencies vs. $\overline{K_v}$ for selected values of rotating speed and taper ratio (shearable beam model)

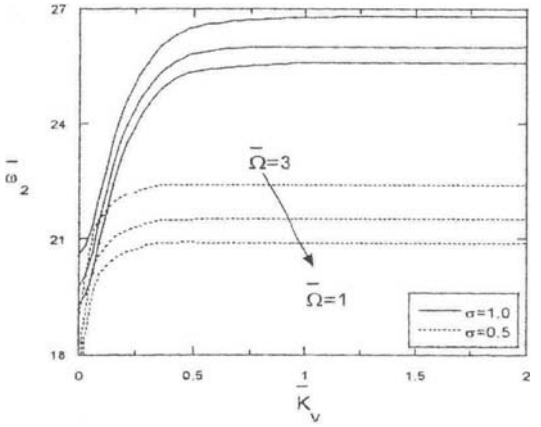

Fig. 10 The counterpart of Fig. 9 for the second closed loop eigenfrequency

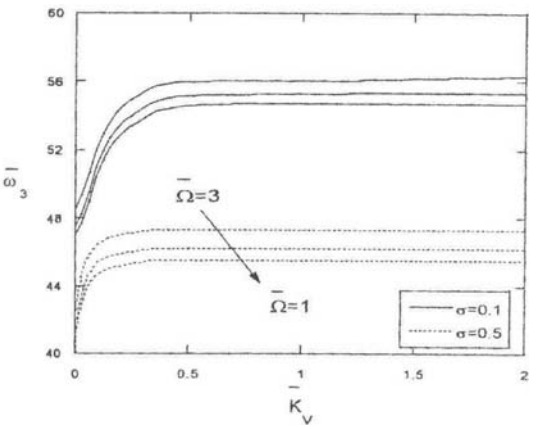

Fig. 11 The counterpart of Fig. 9 for the third closed loop eigenfrequency

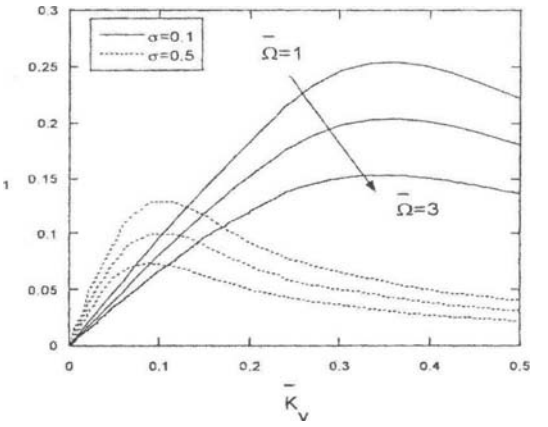

Fig. 12 Piezoelectrically induced damping ζ_1 in flapping vs. $\overline{K_v}$ for two values of the rotational speed and taper ratio (r_0=0.1)

two values of the rotational speed $\overline{\Omega}$, for two values of the taper ratio, and for mass ratio $\varepsilon(\equiv I_{xx}/b_1L^2)=0.05$ and transverse shear $\mu(\equiv a_{33}/L^2 a_{55})=0.007647$. The results reveal the dramatic role played by the implementation of piezo-electric actuation upon the enhancement of eigenfrequencies. As concerns the implications of the taper, these are similar to those already considered in the case of the unactivated rotating beams.

In Fig. 12 the variation of the piezoelectrically induced damping of rotating beam for two values of the taper ratio, vs. the velocity feedback gain is presented. Whereas the effect of the taper ratio is similar to that featured in the case of non-rotating beams (Na and Librescu, 1999), the increase of the rotational speed yields a decrease of the induced damping. This is attributed to the fact that the beam stiffened by the centrifugal effect that increases with the increase of $\overline{\Omega}$, is less prone to induce damping as compared to its less stiff beam counterpart, i.e. of that rotating at lower values of $\overline{\Omega}$.

7. Conclusions

A dynamic structural model of rotating beam of tapered ($0<\sigma\leq 1$) cross-sections was deve-

loped, and the effect of the taper ratio was assessed. Moreover, based upon the converse piezoelectric effect, a distributed actuator methodology aimed at controlling the flapping eigenvibration characteristics of rotating cantilevered thin-walled beams of nonuniform cross-sections was developed. This control is achieved through the piezoelectrically-induced flapwise bending moments at the tip of the beam.

The obtained results reveal that via this control capability it is possible to tune conveniently the eigenfrequencies of the system, and consequently to modify in a beneficial and predictable way the dynamic response characteristics of the structure.

Acknowledgment

The work was supported by a Korea University Grant.

References

Berlincourt, D. A., Curran, D. R. and Jaffe, H., 1964, "Piezoelectric and Piezomagnetic Material and Their Function in Transducers," Physical Acoustics-Principles and Methods, (Eds. W. P. Mason), Vol. 1, Part A, Academic Press, New York and London, pp. 169~270.

Hodges, D. H., 1981, "An approximate Formula for the Fundamental Frequency of a Uniform Rotating Beam Clamped Off the Axis of Rotation," Journal of Sound and Vibration, Vol. 77, No. 11, pp. 11~18.

Librescu, L., Song, O. and Rogers, C. A., 1993, "Adaptive Vibrational Behavior of Cantilevered Structures Modeled as Composite Thin-Walled Beams," International Journal of Engineering Science, Vol. 31, No. 5, pp. 775~792.

Librescu, L., Meirovitch, L. and Song, O., 1994, "Vibration and Static Aeroelastic Instability of Nonuniform Thin-Walled Beam Composite Wings," AIAA/ASME/ASCE/AHS/ASC 35th Structures, Structural Dynamics, and Materials Conference, Paper AIAA-94-1491, Hilton Head, SC.

Du, H., Lim, M. K. and Liew, K. M., 1994, "A Power Series Solution for Vibration of a Rotating Timoshenko Beam," Journal of Sound and Vibration, Vol. 175, No. 4, pp. 505~523.

Park, J. and Yoo, H., 1996, "Bending Vibration of a Pretwisted Rotating Cantilever Beam," *KSME Journal*, Vol. 20, No. 7, pp. 2174~2181.

Librescu, L., Meirovitch, L. and Na, S. S., 1997, "Control of Cantilevers Vibration Via Structural Tailoring and Adaptive Materials," *AIAA Journal*, Vol. 35, No. 8, pp. 1309~1315.

Song, O. and Librescu, L., 1997, "Structural Modeling and Free Vibration Analysis of Rotating Composite Thin-Walled Beams," *Journal of the American Helicopter Society*, Vol. 42, No, pp. 358-369.

Na, S. S. and Librescu, L., 1999, "Dynamic Behavior of Aircraft Wings Modeled as Doubly-Tapered Composite Thin-Walled Beams," P.V.P Vol. 398, Recent Advances in Solids and Structures, Ed. Y. W. Kwon, H. H. Chung, ASME 1999, pp. 59~68.

Na, S. S. and Librescu, L., 2000a, "Modeling and Vibration Feedback Control of Rotating Tapered Beams Incorporating Adaptive Capabilities," PVP-Vol. 415, Recent Advances in Solids and Structures, ASME 2000, pp. 35~43.

Na, S. S. and Librescu, L., 2000b, "Optimal Vibration Control of Thin-Walled Anisotropic Cantilevers Exposed to Blast Loadings," J. of Guidance, Control and Dynamics, Vol. 23, No. 3, pp. 491~500.

Kim, S. and Yoo, H., 2002, "Vibration Analysis of a Rotating Cantilever Plates," *KSME International Journal*, Vol. 16, No. 3, pp. 320~326.

Meirovitch, L., Principles and Techniques of Vibrations, Prentice-Hall, Englewood Cliffs, NJ, 1997.

Tzou, H. S., 1993, Piezoelectric Shells, Distributed Sensing and Control of Continua, Kluwer Academic Publ., Dordrecht/Boston/London.

Librescu, L., Meirovitch, L. and Song, O., 1996, "Integrated Structural Tailoring and Adaptive Materials Control for Advanced Flight Vehicle Structural Vibration," *Journal of Aircraft*, Vol. 33, No. 1, pp. 203~213.

Appendix A

Expressions of stiffness, structural and mass cross-sectional blade characteristics

$$\hat{I}_{yy},\ \hat{I}_{xx},\ \hat{I}_{MM},\ \hat{I}_{LL}=\oint\left\{x^2,\ y^2,\ \left(\frac{dy}{ds}\right)^2,\ \left(\frac{dx}{ds}\right)^2\right\}ds$$

$$I_{yy}=m_0\hat{I}_{yy}+m_2\hat{I}_{MM},\ I_{xx}=m_0\hat{I}_{xx}+m_2\hat{I}_{LL},\ I^o_{xx}=m_2\hat{I}_{xx}$$

$$(m_o,\ m_2)=\sum_{k=1}^{N}\int_{h(k)}\rho^{(k)}(1,\ n^2)\,dn,\ b_1=m_o\oint ds$$

$$a_{22}=\oint(\bar{K}_{11}x^2+\bar{K}_{11}m^2)\,ds,$$

$$a_{33}=\oint(\bar{K}_{11}y^2+\bar{K}_{11}l^2)\,ds,$$

$$a_{44}=\oint(A_{66}l^2+A_{44}m^2)\,ds,$$

$$a_{55}=\oint(A_{66}m^2+A_{44}l^2)\,ds$$

where $l\equiv dx/ds$, $m\equiv dy/ds$

$$\bar{K}_{11}=A_{11}-\frac{A_{12}^2}{11},\ \bar{K}_{11}=D_{11}$$

Herein $(A_{ij},\ D_{ij})=\int_{h(k)}C_{ij}^{(k)}(1,\ n^2)\,dn$ denote shell stretching and bending stiffness quantities, respectively, where the integration is performed over the thickness of both the host and piezoactuator layers.

Appendix B

Several steps aiming at solving the open/closed loop eigenvalue problem.

The method used is based on the extended Galerkin's method (see in this respect Librescu et al. 1997). As a first step, Hamilton's variational principle stating that

$$\int_{t1}^{t2}(\delta T-\delta V+\delta W)\,dt=0,\qquad \delta v_0=\delta\theta_x=0 \text{ at } t_1,\ t_2 \tag{a}$$

is used. Herein T and V denote the kinetic and strain energies, respectively while δW is the virtual work of the nonconservative forces. For the flapping motion only, with consideration of the corresponding T, V, and W in Eq. (a), performing the indicated operations and carrying out usual steps (Meirovitch 1997), it is possible to obtain the boundary value problem. For practical reasons, we discretize the boundary value problem, which amounts to representing v_0 and θ_x by means of series of space dependent trial functions multiplied by time dependent generalized coordinates as

$$v_0(z,\ t)=\phi_1^T(z)\,\mathbf{q}_1(t)$$
$$\theta_x(z,\ t)=\phi_2^T(z)\,\mathbf{q}_2(t) \tag{b}$$

where $\phi_1=[\phi_1\ \phi_2\ \cdots\ \phi_N]^T$ $\phi_2=[\phi_{N+1}\ \phi_{N+2}\ \cdots\ \phi_{2N}]^T$ are vectors of suitable trial functions and $q_1=[q_1\ q_2\ \cdots\ q_N]^T$ $q_2=[q_{N+1}\ q_{N+2}\ \cdots\ q_{2N}]^T$ are vectors of generalized coordinates. Introducing Eq. (b) in Eq. (a), integrating with respect to time, and recognizing that $\delta\mathbf{q}=0$ at $t=t_1,\ t_2$, we obtain the discrete equations of motion

$$\mathbf{M}\ddot{\mathbf{q}}(t)+\mathbf{H}\dot{\mathbf{q}}(t)+\mathbf{K}\mathbf{q}(t)=\mathbf{Q}(t) \tag{c}$$

A solution of Eq. (c) can be obtained conveniently by casting it first in state form. To this end, we introduce the state vector $\mathbf{x}=[\mathbf{q}^T\ \dot{\mathbf{q}}^T]^T$ and adjoin the identity $\dot{\mathbf{q}}=\dot{\mathbf{q}}$. Then, the Eq. (c) becomes

$$\mathbf{x}(t)=\mathbf{A}\mathbf{x}(t)+\mathbf{B}\mathbf{Q}(t) \tag{d}$$

where $\mathbf{A}=\begin{bmatrix}0 & 1\\ -\mathbf{M}^{-1}\mathbf{K} & -\mathbf{M}^{-1}\mathbf{H}\end{bmatrix}$, $\mathbf{B}=\begin{bmatrix}0\\ \mathbf{M}^{-1}\end{bmatrix}$ are coefficient matrices.

For the free vibration problem, the homogeneous solution of Eq. (d) has the form $\boldsymbol{x}=\boldsymbol{X}e^{\lambda t}$ where $\boldsymbol{X}$ is a constant vector and λ is a constant scalar, both generally complex. With this, a standard eigenvalue problem is obtained

$$\mathbf{A}\mathbf{X}=\lambda\mathbf{X} \tag{e}$$

which can be solved for the eigenvalues λ_r and eigenvectors $\mathbf{X}_r$ $(r=1,\ 2,\ \cdots)$.